Clinical Cancer Research

PARP Inhibition Suppresses GR–MYCN–CDK5–RB1–E2F1 Signaling and Neuroendocrine Differentiation in Castration-Resistant Prostate Cancer

Bo Liu[1], Likun Li[1], Guang Yang[1], Chuandong Geng[1], Yong Luo[1], Wenhui Wu[2], Ganiraju C. Manyam[2], Dimitrios Korentzelos[1], Sanghee Park[1], Zhe Tang[1], Cheng Wu[1], Zhenyang Dong[1], Michael Sigouros[3], Andrea Sboner[4,5,6], Himisha Beltran[7], Yu Chen[3,8,9], Paul G. Corn[1], Michael T. Tetzlaff[10], Patricia Troncoso[10], Bradley Broom[2], and Timothy C. Thompson[1]

Abstract

Purpose: In this study, we addressed the underlying mechanisms for the association between enzalutamide (ENZ) treatment and neuroendocrine prostate cancer (NEPC), and the critical involvement of MYCN, and loss of RB1 function in neuroendocrine differentiation (NED) of prostatic epithelial cells, and the development of NEPC. We further sought to determine whether PARP inhibition could suppress NEPC, and to identify molecular determinants of this therapeutic activity.

Experimental Design: We used a novel prostate cancer patient–derived xenograft (PDX) treatment model, prostatic adenocarcinoma and NEPC cell lines, an NEPC organoid line, and NEPC xenograft models to address the mechanistic basis of ENZ-induced NED, and to analyze suppression of NED and NEPC growth by PARP inhibition.

Results: We identified an ENZ treatment–associated glucocorticoid receptor (GR)–MYCN–CDK5–RB1–E2F1 signaling pathway that drives NED in prostatic adenocarcinoma PDX and cell line models. Mechanistically, long-term ENZ treatment transcriptionally upregulates signaling of the GR–MYCN axis, leading to CDK5R1 and CDK5R2 upregulation, Rb1 phosphorylation, and N-Myc–mediated and E2F1-mediated NED gene expression. Importantly, olaparib (OLA) or talazoparib (TALA) suppressed these activities, and the combination of OLA and dinaciclib (DINA), an inhibitor of CDK2 and CDK5, which also inhibits Rb1 phosphorylation, suppressed NED and significantly improved therapeutic efficiency in NEPC cells *in vitro* and in NEPC tumors *in vivo*.

Conclusions: The results of our study indicate an important role of GR–MYCN–CDK5R1/2–RB1–NED signaling in ENZ-induced and PARP inhibitor–suppressed NEPC. We also demonstrated efficacy for OLA+DINA combination therapy in NEPC xenograft models.

Introduction

Hormonal therapy remains the principal treatment for metastatic prostate cancer, including disease that continues to progress following initial androgen deprivation to a lethal phenotype known as castration-resistant prostate cancer (CRPC). Novel second-generation androgen signaling inhibitors, such as abiraterone (ABI) and enzalutamide (ENZ), which maximally suppress androgen signaling, increase survival by 4 and 4.8 months for patients with metastatic CRPC, respectively (1, 2). Despite the moderate benefit of these agents, their success in treating CRPC has been hampered by emergence of drug resistance. Notably, glucocorticoid receptor (GR), a steroid receptor

[1]Department of Genitourinary Medical Oncology, The University of Texas MD Anderson Cancer Center, Houston, Texas. [2]Department of Bioinformatics and Computational Biology, The University of Texas MD Anderson Cancer Center, Houston, Texas. [3]Department of Medicine, Weill Cornell Medical College, New York, New York. [4]Englander Institute for Precision Medicine, Weill Cornell Medical College and New York Presbyterian Hospital, New York, New York. [5]Department of Pathology and Laboratory Medicine, Weill Cornell Medical College, New York, New York. [6]Institute for Computational Biomedicine, Weill Cornell Medical College, New York, New York. [7]Department of Medical Oncology, Dana Farber Cancer Institute, Harvard Medical School, Boston, Massachusetts. [8]Human Oncology and Pathogenesis Program, Memorial Sloan Kettering Cancer Center, New York, New York. [9]Department of Medicine, Memorial Sloan Kettering Cancer Center, New York, New York. [10]Department of Pathology, The University of Texas MD Anderson Cancer Center, Houston, Texas.

Note: Supplementary data for this article are available at Clinical Cancer Research Online (http://clincancerres.aacrjournals.org/).

B. Liu and L. Li contributed equally to this article.

Current address for Bo Liu: Department of Oncology, Tongji Hospital, Tongji Medical College, Huazhong University of Science and Technology, Wuhan, Hubei, China.

T.C. Thompson is a lead contact.

Corresponding Author: Timothy C. Thompson, The University of Texas MD Anderson Cancer Center, 1515 Holcombe Boulevard, Unit 18-3, Houston, TX 77030. Phone: 713-792-9955; Fax: 713-792-9956; E-mail: timthomp@mdanderson.org

Clin Cancer Res 2019;25:6839–51

doi: 10.1158/1078-0432.CCR-19-0317

Translational Relevance

Emerging evidence has revealed an association between hormonal treatment and neuroendocrine prostate cancer (NEPC), and the critical involvement of MYCN, and loss of RB1 function in the development of NEPC. However, the mechanisms that underlie enzalutamide (ENZ) treatment–associated neuroendocrine differentiation (NED) and the development of NEPC remain to be addressed. The GR–MYCN–CDK5–RB1–E2F1 signaling pathway identified in our study defines a transcriptional regulatory mechanism that underlies the transition from ENZ resistance to NED, in the development of NEPC. This mechanism links ENZ resistance in prostatic adenocarcinoma to NED through GR-induced MYCN, and reveals CDK5-driven inactivation of intact Rb1 as a driver of E2F1-regulated NED gene expression. Our results further demonstrate that PARP inhibition suppresses the GR–MYCN–CDK5–RB1–E2F1 signaling pathway, and direct MYCN and E2F1 induction of NED, and that the combination of PARP inhibition and Rb-associated CDK inhibition may be a viable strategy toward effective clinical treatment of NEPC.

family member, was found to be overexpressed in AR signaling inhibitor resistant tumors (3).

Primary localized prostate cancer almost exclusively exhibits adenocarcinoma (Ad) morphology, whereas neuroendocrine prostate cancer (NEPC) more commonly arises after hormonal therapy (4), and is more prevalent in CRPC (5, 6). A recent prospective study demonstrated that prostate cancer from patients treated with AR signaling inhibitors transitioned from Ad prostate cancer into NEPC at a higher rate than those who were not treated with these agents (7). Although platinum-based chemotherapy is active in NEPC, responses are short-lived and novel therapeutic approaches are needed.

The phenotypic conversion from Ad prostate cancer to NEPC has been associated with specific genetic lesions including overexpression and genomic amplification of MYCN (encoding N-Myc oncoprotein; refs. 5, 8). MYCN is overexpressed in the majority of NEPC but also in up to 20% of CRPC without NEPC morphology (5, 9). Furthermore, a recent study demonstrated that MYCN could drive the initiation and maintenance of NEPC from prostate epithelial cells (10). However, the mechanisms involved in androgen signaling inhibitor-treatment associated MYCN induction and MYCN-driven NEPC have not been defined.

The E2F family transcription factors play an essential role in cancer cell proliferation by regulation of the cell-cycle G_1–S transition. The activities of E2F proteins are restricted by the retinoblastoma protein 1, encoded by retinoblastoma susceptibility gene *RB1* (11). E2F proteins are released from Rb1 and activated for gene transcription when Rb1 is inactivated by CDK-mediated hyperphosphorylation. Dysfunctional Rb1 has been implicated in several major cancers, and loss of *RB1* has been identified as a major molecular event associated with lineage plasticity of aggressive variant prostate cancer and treatment-related NEPC (12–14). Recent publications also demonstrate that loss of Rb1 and p53 are required to induce proliferation and lineage plasticity during the conversion of an epithelial lineage into a neuroendocrine lineage in the development of NEPC in genetically engineered mouse models and a human-mouse tissue recombination model (15–17). Thus, inactivation of RB1 and p53 appear to be critical for lineage plasticity—related Ad prostate cancer–NEPC transition. However, the mechanisms involved in this process remain elusive.

PARP inhibitors are promising therapeutic agents that show synthetic lethality against many types of cancer with BRCA1 or BRCA2 deficiencies (18, 19). Targeting PARP together with specific DNA damage response (DDR) pathways exposed previously unrecognized therapeutic vulnerabilities in CRPC models (20–22). However, whether PARP inhibitors can specifically suppress or alter the course of NED is not known.

Overall, emerging evidence has revealed an association between hormonal treatment and NEPC, and the critical involvement of MYCN and RB1 in NED of prostatic epithelial cells and the development of NEPC. However, their exact roles and the mechanisms that underlie ENZ treatment—associated NED and the development of NEPC remain to be addressed. Our results herein introduce a GR–MYCN–CDK5–RB1–E2F1–NED signaling pathway, and reveal the underlying molecular mechanisms for suppression of ENZ-induced NED by PARP inhibition.

Materials and Methods

Cell lines, patient-derived xenografts, and reagents

LNCaP C4-2b cells were maintained in RPMI1640 cell culture medium supplemented with 10% FBS. C4-2b-ENZR cells were generated by long-term ENZ treatment with incremental increase of ENZ concentrations in each passage (with 0.5 μmol/L intervals up to 3 and 1 μmol/L intervals afterward up to 10 μmol/L). The resulting C4-2b-ENZR cells were maintained in RPMI1640 medium supplement with 10% FBS plus 10 μmol/L ENZ. NCI-H660 cells were purchased from ATCC, and maintained in suggested culture medium. MSKCC PCa4 organoids were maintained in complete human media as described previously (23). MDA prostate cancer patient-derived xenograft (PDX) 133-4 and MDA prostate cancer PDX 144-13C were developed in the "Prostate Cancer Patient Derived Xenografts Program" in the department of Genitourinary Medical Oncology, MD Anderson Cancer Center and the David H. Koch Center for Applied Research of Genitourinary Cancers following published methods (24). LNCaP C4-2b was validated by short tandem repeat DNA fingerprint with the AmpFlSTR Identifier PCR Amplification Kit (Themo Fisher Scientific) in MD Anderson's Characterized Cell Line Core Facility. Genomic mutation/deletion analysis for all cell lines and PDX tumors was performed by targeted DNA sequencing (Supplementary Fig. S1; Supplementary Table S1). ENZ (S1250), olaparib (KU-0059436), talazoparib (TALA; BMN673), dinaciclib (DINA; SCH727965), and dexamethasone (S1322) were purchased from Selleck Chem. Cort-108297 (L13976) was from Advanced Chem Blocks. Antibodies are listed in Supplemental Experimental Procedures.

Generation of treatment resistance xenografts

A schematic depicting of model generation is shown in Fig. 1A. Detailed protocol is available in Supplementary Experimental Procedures.

RNA-Seq analysis

Total RNA was extracted from cell lines, tumor tissues, and from micro-dissected paraffin-embedded MDA prostate cancer PDX133-4 tumor sections and proceed to RNA-Seq (see

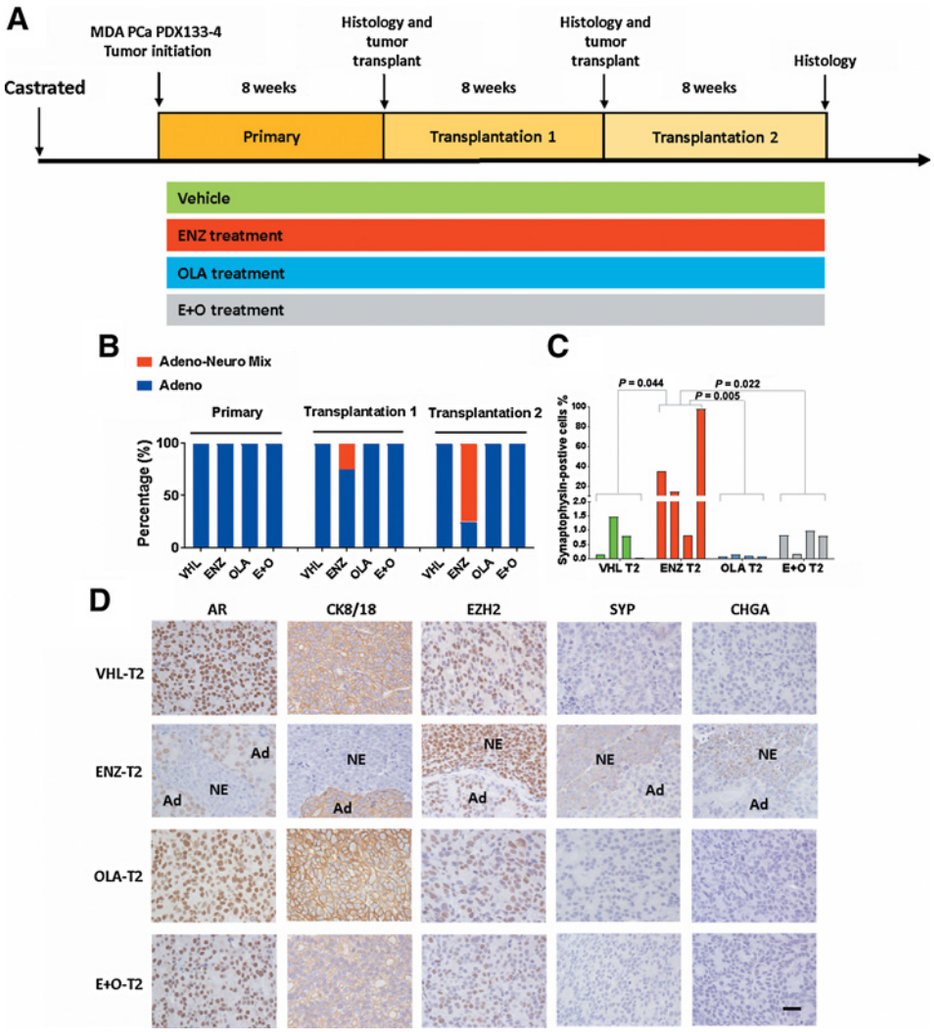

Figure 1.
ENZ promotes and OLA inhibits NE transition in MDA prostate cancer PDX133-4 model. **A,** Experiment schematic depiction. See detail in Supplementary Materials and Methods. **B,** Pathologic analysis demonstrated 25% tumors in ENZ-T1 and 75% tumors in ENZ-T2 group were mixed adeno-neuroendocrine (Ad-NE) carcinomas, all the other tumors remained Ad phenotype. Mixed Ad-NE carcinomas were identified by HE staining and histologic criteria. **C,** Synaptophysin IHC analysis of T2 tumors. Quantitation of synaptophysin-positive cells was performed by using an image analysis system (Nikon Eclipse 90i) and the Nikon NIS-Elements version 3.0 software on systematically scanned tumor slides. **D,** Representative images of AR, CK8/18, EZH2, SYP, and CHGA IHC staining of T2 tumors. Scale bar represents 50 μm.

Supplementary Experimental Procedures). Xenograft samples were assayed by RNA-Seq (Illumina) to analyze the transcriptome. Xenome was used to classify the xenograft sequence data into corresponding tumor and mouse reads (25). The raw reads from tumor were aligned to the Human reference genome (hg19) using Tophat2 transcriptome alignment tool (26). Samtools and HTseq software were utilized to summarize the gene expression counts from alignment data (27, 28).

Differential gene expression analysis and GSEA pathway analysis

Differential expression analysis was performed on the read counts with R package DESeq2 (29). Significant differentially expressed genes were defined by false discover rate of 0.01 and log fold change threshold of 1.5. Gene set enrichment analysis (GSEA) was performed using the Hallmark pathway database (29). Common leading edge genes were extracted by comparative analyses of GSEA results in pathways of interest. The gene expression of common significant differentially expressed and leading edge genes were illustrated by heatmaps. The DDR-M gene list was developed as described previously (22). The expression of DDR-M genes of interest was extracted from normalized data matrix. Two-sample *T* test, comparing Ad versus NE, was performed and *P* values were adjusted by Benjamini–Hochberg procedure.

RT-qPCR analysis

Total RNA in cells were extracted by TRIzol reagent (Thermo Fisher Scientific) and reversely transcribed to cDNA using high capacity cDNA Reverse Transcription Kit (Thermo Fisher Scientific). qRT-PCR was conducted using fast SYBR green master mix (Thermo Fisher Scientific). $2^{-\Delta\Delta Ct}$ method was used to evaluate relative mRNA expressions compared with controls. The primer sequences are listed in Supplementary Table S8.

Nanostring analysis

Gene expression analysis of a panel of 361 genes was performed using a custom nanostring assay described previously (30). AR score was calculated using an AR signaling gene signature described in Hieronymous and colleagues (31), with LNCaP cell line as reference. NEPC score was calculated using gene signature described in Beltran and colleagues (8), with NEPC cell line NCI-H660 as reference. Cell lines (C4-2b and C4-2b-ENZR) were compared under the described experimental conditions and with

a cohort of human tumors—D70 localized prostate adenocarcinoma, 15 CRPC, and 22 NEPC, described in refs. 8 and 30.

Protein immunoblot analysis

Total proteins in cells were extracted by NP-40 lysis buffer with proteinase inhibitor cocktail (Roche) and phosphatase inhibitor cocktail (Millipore), and Western blotting analysis was performed as described in standard protocol.

siRNA transfection

Cells were seeded 1 day before siRNA transfection, and were transfected with 20 nmol/L siRNA using the Lipofectamine RNAiMax transfection reagent (Themo Fisher Scientific). RNA and protein extracts were prepared and biological assays were performed 48 hours after siRNA transfection. siRNA sequences are listed in Supplementary Table S9.

ChIP-qPCR assays

ChIP-qPCR assays were performed using the SimpleChIP-Plus Enzymatic Chromatin IP Kit (Cell Signaling Technology) according to manual instructions. Briefly, cells were fixed and chromatins were prepared. The chromatins were sonicated and immunoprecipitated using protein specific antibodies to GR, N-Myc, or E2F1. The immunocomplex were captured by protein G beads, washed, and eluted. After reverse-crosslink, the chromatin DNAs were purified and used as the template in qPCR analysis to detect the recruitment of proteins. Normal rabbit IgG (Cell Signaling Technology) was used as negative control. The primers used in qPCR are listed in Supplementary Table S10.

MTS assay

Following the manual, MTS assay was performed using CellTiter 96 AQueous One Solution Cell Proliferation Assay (Promega).

Colony assay

Cells were seeded into 6-well plates at 2×10^4/well and treated with 1 μmol/L ENZ for up to 2 weeks for colony formation. Cell culture medium containing ENZ or DMSO was renewed every 3 days. Afterwards, colonies were fixed with cold methanol and stained with 0.5% crystal violet. The number of colonies was counted and imaged with a microscope using NIS-Elements AR2.30 software (Nikon).

Xenograft model

Aliquots of 2×10^6 NCI-H660 cells in 100 μL of PBS: Matrigel (1:1) were injected subcutaneously into the right flanks of athymic male mice. Tumors were allowed to grow until they reached 50 mm^3 before they were randomly distributed and treated. Equal-sized MDA prostate cancer PDX144-13C tumor fragments were implanted subcutaneously into previously castrated SCID mice (Charles River Laboratories) as described previously (22). When the tumor volume reached 30 to 50 mm^3, the mice were randomly distributed and treated. In both tumor models, mice were randomly divided to receive vehicle control [20% (2-hydroxypropyl)-β-cyclodextrin in PBS], OLA (40 mg/kg/day, 5 days each week, i.p.), DINA (30 mg/kg/day, 2 days each week, i.p.), or combination OAL and DINA for 21 days. Subcutaneous tumors were measured twice a week after the initiation of the treatment. All animal experiments were conducted in accordance with accepted standards of humane animal care approved by MDACC IACUC.

IHC and ISH analysis

Primary antibodies to AR (Santa Cruz Biotechnology), CK8/18 (Abcam) Synaptophysin (Abcam), EZH2 (Abcam), Chromogranin A (Abcam), and GR (Cell Signaling Technology) were used for immunostaining on cell line samples and formalin-fixed paraffin-embedded tissue slides from the PDX models. MYCN mRNA expression was analyzed by ISH using a human MYCN probe (VA1-18174) and the view RNA-ISH system from Affymetrix.

Immunofluorescence analysis

Cells were seeded on coverslips in 24-well plates. After treatments cells were rinsed with PBS, and fixed 4% PBS-buffered formaldehyde for 8 minutes; followed by incubation in 0.5% Triton-X100 in PBS for 10 minutes to enhance antibody penetration. After a 20 minute-blocking in Dako protein block (Dako) for 20 minutes, the cells were incubated with primary antibodies for 1 hour, followed by incubation with an Alexa Fluor 488- or Alexa Fluor 594-conjugatged secondary antibody (Invitrogen) for 40 minutes. Specificity of immunofluorescence was validated by replacing primary antibody with PBS.

Statistical analysis

Data were presented as the mean ± SEM. The Wilcoxon rank-sum test was used for data with nonnormal distributions or data with small sample sizes such as qRT-PCR analyses, ChIP assay, MTS assay, colony assay, flow cytometry assay, and scratch assay. ANOVA *t* test was used for analysis of tumor growth and tumor wet weights. *P* value <0.05 was considered statistically significant.

Results

ENZ promotes and OLA suppresses NED in MDA prostate cancer PDX133-4

To analyze ENZ resistance over an extended time period, we implanted equal-sized MDA prostate cancer PDX133-4 tumor fragments subcutaneously into precastrated male SCID mice and treated them with vehicle control (VHL), ENZ, OLA, or ENZ+OLA. Targeted genomic DNA sequencing revealed a *TP53* point mutation (C141Y), and negative p53 expression (Supplementary Fig. S2A), but no *RB1* mutation in this PDX tumor model (Supplementary Fig. S1 and S2B; Supplementary Table S1). Analysis of the functionality of the TP53 C141Y point mutation suggested severe conformational changes in the mutant p53 protein (32). After primary treatment, tumor pieces from each of the experimental groups were transplanted into precastrated male SCID mice and the treatments were repeated for 2 rounds of transplantation (T1 and T2; Fig. 1A). Pathologic analysis of these tumors revealed: 1 of 4 tumors in ENZ-T1 group demonstrated a mixed, but well demarcated, Ad and NE morphology (NE content 1.56%; Supplementary Table S2), 3 of 4 tumors in ENZ-T2 group demonstrated similar mixed Ad and NE morphology (with NE content ranging from 21% to 96%; Supplementary Table S2); and surprisingly, all VHL-, OLA-, and ENZ+OLA-treated T1 and T2 tumors remained Ad phenotype after T1 and T2 (Fig. 1B; Supplementary Table S3). IHC analysis of T2 tumors revealed that expression of synaptophysin (SYP, a NED marker)-positive cells were significantly increased in ENZ-T2 tumors compared with VHL-, OLA-, or ENZ+OLA-T2 tumors (Fig. 1C

and D). Furthermore, AR and cytokeratin 8/18 (CK8/18, epithelial cell markers) were negative or very low, and EZH2 (chromatin remodeling marker), SYP, and chromogranin A (CHGA, another NE marker) were markedly higher in the NE regions of ENZ-T2 tumors compared with adjacent Ad tissues (Fig. 1D).

Suppression of AR signaling pathway and upregulation of GR and MYCN in NED and NEPC tumors

Using NE scores, derived from RNA sequencing data and defined by the expression of 70 NE-related classifier genes (8), we identified 2 ENZ-T2 NE tumors with NE scores >0.4 (cut off established by Beltran and colleagues); 1 ENZ-T1 tumor and 3 ENZ-T2 tumors with NE scores >0.2 and <0.4; and all VHL, OLA, and ENZ+OLA-treated T1 and T2 tumors had NE scores <0.2 (Supplementary Table S4; Fig. 2A). Because the majority of pathologically defined Ad tumors had NE scores <0.2, and an NE score >0.4 was previously used as a cut off for NEPC (8), we defined tumors with NE scores >0.2 and <0.4 as transition (TR) tumors. Thus, on the basis of molecular criteria, our results included 1 Ad→TR mixed tumor in ENZ-T1, as well as 1 Ad→TR and 2 TR→NE mixed tumors in ENZ-T2 (Fig. 2A). Global gene expression analysis of T2 tumors revealed 2,700 common genes significantly altered between 2 comparisons: ENZ-NE vs. VHL and ENZ-NE vs. ENZ-Ad. As shown in the heatmap for the expression patterns of these genes in T2 tumors, ENZ-TR and ENZ-NE tumors are distinctly different from those of ENZ-Ad and other Ad tumors (Fig. 2B). Similarly, expression of 70 NED-related classifiers gene also formed a distinct pattern that clearly distinguish ENZ-TR and ENZ-NE tumors from Ad tumors (Fig. 2C).

Specifically, we found that the expression of AR and AR target genes was significantly downregulated in ENZ-NE compared with other treatment groups (Fig. 2D–I). Interestingly, although AR mRNA levels in ENZ-TR were not significantly different from VHL (Fig. 2E), analysis of AR target gene expression (Fig. 2D) and GSEA leading edge analysis of androgen response pathway (Fig. 2F) revealed that AR target gene expression was markedly diminished in ENZ-TR compared with VHL. More pronounced suppression of androgen response genes/pathway was found in the ENZ-NE group when it was compared with VHL (Fig. 2D–G), ENZ-Ad (Fig. 2D–H), and ENZ-TR (Fig. 2D–I).

Analysis of NR3C1 (GR) and MYCN expression showed that mRNA levels of GR and MYCN were significantly or markedly higher in ENZ-TR and ENZ-NE compared with VHL and ENZ-Ad (Fig. 2J and K). Interestingly, elevated GR and MYCN expression was not observed in OLA and ENZ+OLA tumors which maintained GR and MYCN mRNA at levels similar to those in VHL group (Fig. 2J–K). Correlation analysis indicated that GR and MYCN mRNA expression was positively correlated in MDA prostate cancer PDX133-4 tumor samples (Fig. 2L) and a published dataset of tumor samples from patients treated with AR signaling inhibitors (Fig. 2M; ref. 7). IHC detection of GR and RNA *in situ* hybridization of MYCN in these tumor samples showed increased frequency of GR-positive and MYCN-positive cells in the NE element of MDA prostate cancer PDX133-4 ENZ-T2 tumors (Fig. 2N).

GR transcriptionally regulates MYCN

To analyze the molecular mechanisms that underlie this ENZ treatment-associated NED, we generated an ENZ-resistant (ENZR) prostate cancer cell line (C4-2b-ENZR) from C4-2b (AR-positive and ENZ-sensitive) through long-term ENZ treatment, using incremental increases in ENZ concentration. C4-2b-ENZR cells could be distinguished from its parental cells by morphologic characteristics that included smaller size, and reduced nuclear circularity and increased nucleus/cytoplasm ratio (Supplementary Fig. S3A and S3B). Targeted genomic DNA sequencing revealed 2 gained *TP53* mutations (one frame shift mutation P72fs and a point mutation Q331R) but no *RB1* mutation in C4-2b-ENZR (Supplementary Fig. S1; Supplementary Table S1). Compared with parental C4-2b cells, C4-2b-ENZR cells demonstrated increased clonal growth during treatment/selection (Supplementary Fig. S3A, middle; Supplementary Fig. S3E and S3F), resistance to ENZ treatment (Supplementary Fig. S3E and S3F), and increased cell proliferation (Supplementary Fig. S3F). Western blotting analysis showed reduced expression of AR, and elevated expression of AR-V7, GR, N-Myc, and NED genes including SYP and CHGA (Supplementary Fig. S3D). In addition, IHC confirmed reduced nuclear AR and markedly increased nuclear GR in C4-2b-ENZR compared with parental cells C4-2b (Supplementary Fig. S4A and S4B). Knockdown of AR led to significantly increased GR expression in C4-2b, C4-2b-ENZR, and NCI-H660, an NEPC cell line, supporting a mechanism of GR upregulation that involves inhibition of AR signaling (Supplementary Fig. S4C; Supplementary Table S1). Interestingly, AR and NEPC scores for C4-2b and C4-2b-ENZR cell lines demonstrated reduced AR score, but an increased NEPC score for C4-2b-ENZR cells compared with C4-2b cells (Supplementary Fig. S5).

Notably, we found that GR knockdown resulted in downregulation of MYCN mRNA (Fig. 3A) and protein (Fig. 3B) in the same 3 cell lines. Furthermore, in line with these findings, GR antagonist CORT-108297 (CORT) treatment downregulated N-Myc in these cell lines (Fig. 3C). These results suggested that GR may transcriptionally regulate MYCN. We identified a glucocorticoid response element (GRE) DNA sequence (BS1; Fig. 3D, Supplementary Table S5) in the MYCN promoter region, and ChIP-qPCR assay results confirmed the *in vivo* recruitment of GR protein to BS1 of the MYCN promoter in these prostate cancer cells. More interestingly, compared with C4-2b cells, the recruitment of GR protein to BS1 is significantly increased in C4-2b-ENZR and NCI-H660 cells in which expression of GR is upregulated (Fig. 3E). Thus, taken together, we identified an intact mechanism involving GR-driven expression of the MYCN gene (GR–MYCN axis) in the ENZ-resistant CRPC cell line C4-2b-ENZR and NCI-H660 cells.

N-Myc- and RB1-dependent, CDK5 R1/R2- and E2F1-mediated NED signaling pathway

In our previous studies, we found that MYCN regulated the DDR pathway in NEPC (22). These findings led us to conduct a bioinformatics analysis for the common significant DDR-mitotic (DDR-M) genes (22) in MDA prostate cancer PDX133-4 tumor samples and tumor samples from 2 published datasets (7, 8). Our analysis generated 54 common significant DDR-M genes from these 3 datasets (Supplementary Tables S6 and S7; Fig. 3F). The top common significant DDR-M genes included CDK5R2 and CDK5R1, which are activators of CDK5 and highly implicated in NED (33–36), and E2F1. Bioinformatics analysis showed significantly higher mRNA expression of CDK5R1, CDK5R2, and E2F1 in ENZ-TR and ENZ-NE tumors compared with tumors from other treatment groups in MDA prostate cancer PDX133-4 (Fig. 3G–I), and CDK5R1, CDK5R2, and E2F1 mRNA expression

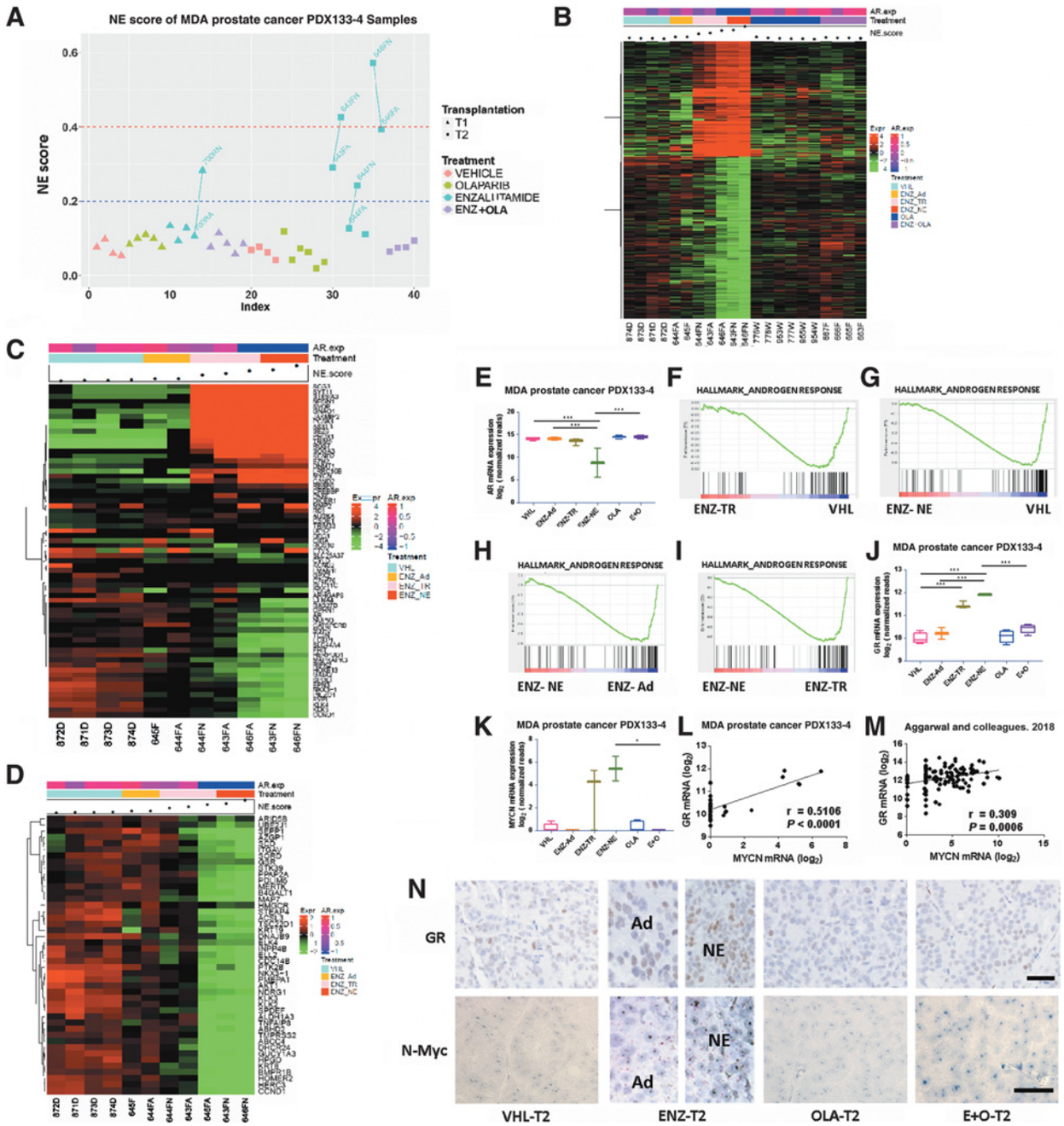

Figure 2.

Downregulation of AR response gene pathway and upregulation of GR and MYCN in NE transition tumors. **A,** NE score plot of PDX133-4 T1 and T2 tumor samples. Ad and NE contents were micro-dissected from mixed Ad-NE carcinomas, designated as "A" and "N," respectively, and processed for RNA-Seq analysis. Using Beltran's CRPC-Neuro reference vector, the Pearson correlation coefficients (NE scores) of T1 and T2 MDA prostate cancer PDX 133-4 tumors were calculated and plotted. T1, triangle; T2, square; VHL, red; OLA, green; ENZ, blue; ENZ+OLA, purple. **B,** Common significant (FDR: 0.01, log2FC: 1.5) differentially expressed genes from 2 comparisons, ENZ-NE vs. ENZ-Ad and ENZ-NE vs. VHL, were illustrated in the heatmap. **C,** Expression of Beltran 70 classifier genes in MDA prostate cancer PDX133-4 RNA-Seq dataset. **D,** Heatmap of AR target gene expression in MDA prostate cancer PDX133-4 T2 samples. **E,** AR gene expression in MDA prostate cancer PDX133-4 T2 samples. **F,** GSEA plot showing androgen response pathway genes positively correlated with VHL samples compared with ENZ-TR samples. **G,** VHL samples compared with ENZ-NE samples. **H,** ENZ-Ad samples compared with ENZ-NE samples. **I,** ENZ-TR samples compared with ENZ-NE samples. **J,** GR gene expression of T2 samples in MDA prostate cancer PDX133-4 tumors. **K,** MYCN gene expression of T2 samples from MDA prostate cancer PDX133-4 tumors. **L,** Correlation between GR and MYCN mRNA expression in MDA prostate cancer PDX133-4 tumors. **M,** Correlation between GR and MYCN mRNA expression in Aggarwal and colleagues' dataset. **N,** GR IHC and MYCN ISH analysis of T2 samples from MDA prostate cancer PDX133-4 tumors. *, $P < 0.05$; **, $P < 0.01$; ***, $P < 0.001$. Scale bar represents 40 μm.

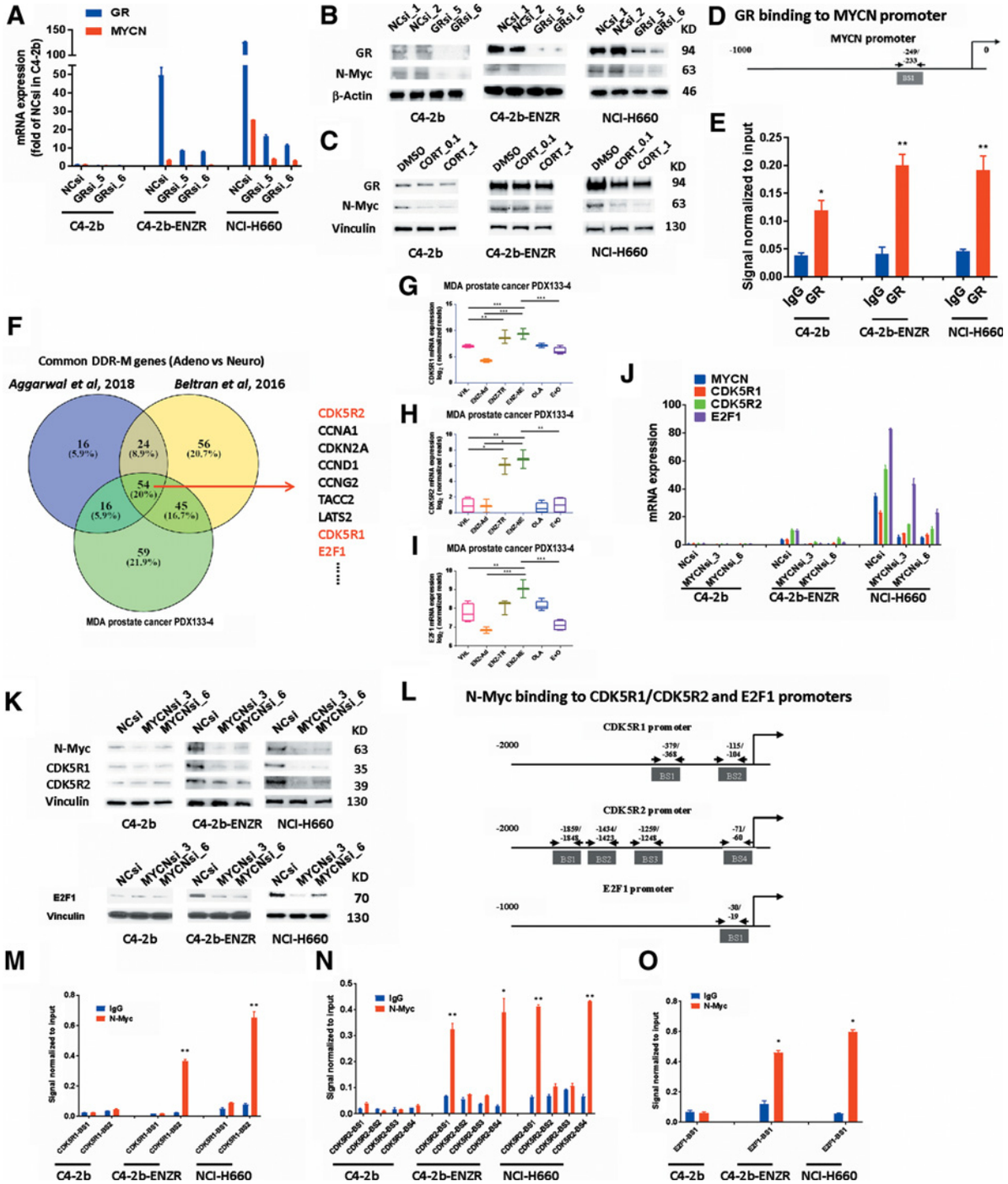

Figure 3.

GR transcriptionally regulates MYCN expression, and N-Myc transcriptionally regulates CDK5R1, CDK5R2, and E2F1 expression. **A** and **B,** Effect of GRsi on mRNA and protein expression of GR and MYCN in C4-2b, C4-2b-ENZR, and NCI-H660 cells. **C,** Effect of GR antagonist CORT-108297 (CORT) on N-Myc protein expression. **D,** Predicted GR binding sites on MYCN promoter according to JASPAR database. **E,** ChIP-PCR assay testing the direct binding of GR to MYCN promoter in C4-2b, C4-2b-ENZR, and NCI-H660. **F,** Common significant DDR-M genes comparing NE samples (NE score > 0.4) with Ad samples (NE score < 0.2) in MDA prostate cancer PDX133-4, and the Beltran and colleagues', and Aggarwal and colleagues' datasets. Note that CDK5R2, CDK5R1, and E2F1 are among the top significant genes (Supplementary Table S4). **G–I,** CDK5R1, CDK5R2, and E2F1 gene expression in MDA PCa PDX133-4 T2 tumors. **J** and **K,** Effect of MYCNsi on mRNA and protein expression of MYCN, CDK5R1, CDK5R2, and E2F1 in C4-2b, C4-2b-ENZR, and NCI-H660 cell lines. **L,** Predicted MYCN binding sites on CDK5R1, CDK5R2, and E2F1 promoter according to JASPAR database. **M–O,** ChIP-qPCR assays testing the direct binding of MYCN to CDK5R1, CDK5R2, and E2F1 promoters in C4-2b, C4-2b-ENZR, and NCI-H660. *, $P < 0.05$; **, $P < 0.01$; ***, $P < 0.001$.

was positively correlated to MYCN mRNA expression in MDA prostate cancer PDX133-4 (Supplementary Fig. S6A–S6C) and in Beltran and colleagues' dataset (Supplementary Fig. S64D–S64F). GSEA leading edge analysis indicated E2F target gene being a top altered pathway after long-term ENZ treatment in MDA prostate cancer PDX133-4 (Supplementary Fig. S6G–S6I). On the basis of these results, we decided to test the possibility that MYCN regulates CDK5R1/R2 and E2F1 expression. MYCN knockdown using siRNA markedly reduced CDK5R1, CDK5R2, and E2F1 expression of both mRNA (Fig. 3J) and protein (Fig. 3K) in C4-2b, C4-2b-ENZR, and NCI-H660 cells. We identified 2 consensus N-Myc binding sites in the CDK5R1 promoter, 4 consensus N-Myc binding sites in the CDK5R2 promoter and an N-Myc binding site on E2F1 promoter (Fig. 3L; Supplementary Table S5). Thus, we designed primers spanning these E-box DNA regions and utilized ChIP-qPCR assays to detect the *in vivo* recruitment of N-Myc at the promoters of CDK5R1, CDK5R2, and E2F1 genes in prostate cancer cells. Our results showed that N-Myc was recruited to the CDK5R1 promoter (BS2), the CDK5R2 promoter (BS1 and BS4), and the E2F1 promoter (BS1) *in vivo* in C4-2b-ENZR and H660 cells, but N-Myc recruitment was not seen in C4-2b cells (Fig. 3M–O).

Correlation analysis revealed that mRNA expressions of CHGA, SYP, and neuron-specific enolase (NSE) were positively correlated with mRNA expression of CDK5R1, CDK5R2, and E2F1 in MDA prostate cancer PDX133-4 (Supplementary Fig. S7A), and tumor samples from 2 different published datasets (Supplementary Fig. S7B and S7C; refs. 7, 8). Although *CDK5R1* knockdown seemed to reduce only SYP, but not CHGA and NSE expression (Fig. 4A), *CDK5R2* and *E2F1* knockdown resulted in markedly reduced expression of all 3 NED genes, CHGA, SYP, and NSE (Fig. 4B and C), suggesting that CDK5R2 may function as primary activator of CDK5 in regulation of NED gene expression, and E2F1 may be involved in transcriptional regulation of NED genes. Because RB1 is a known phosphorylation target of CDK5 (37–39) and a crucial regulator of E2F1 (11), and loss of *RB1* function has been linked to NE development (40, 41), and to lineage plasticity of aggressive variant prostate cancer and treatment-related NEPC (12–14), we speculated that RB1 may play a critical role downstream of CDK5, and function as a component of the underlying molecular pathway for N-Myc-dependent, CDK5R1/R2-mediated, and E2F1-mediated NED. Inhibition of CDKs by DINA (targets CDK2, CDK5, CDK1, and CDK9, with reduced IC_{50} to CDK2 and CDK5) strongly inhibited Rb1 phosphorylation and CHGA, SYP, and NSE expressions (Fig. 4D). In contrast, knockdown of RB1 using siRNA markedly increased expression of these NED markers (Fig. 4E). We identified several consensus E2F1 binding elements in the promoter DNA sequences of CHGA, SYP, and NSE (ENO2; Fig. 4F; Supplementary Table S5). Using ChIP-qPCR assays, we confirmed the functional recruitment of E2F1 at the promoter of CHGA, SYP, and NSE genes, with binding preference to BS2 of CHGA, BS1 of SYP, and BS1 of NSE (Fig. 4G and H), which is consistent with the elevated mRNA expression of these genes observed in C4-2b-ENZR and NCI-H660 cells. We further confirmed a direct N-Myc-NED regulation pathway that was reported in a previous publication (Supplementary Fig. S8; Supplementary Table S5; ref. 5). Analysis of MYCN, CDK5R1, CDK5R2, E2F1, CHGA, SYP, and NSE mRNAs in 2 published datasets showed increased expressions in all cases, suggesting a biological relationship (Fig. 4J and K). Taken together, these data suggest that upregulation of N-Myc in ENZ-TR and ENZ-NE effectively activates CDK5 through transcriptional upregulation of CDK5R1 and CDK5R2; CDK5R1 and CDK5R2 (through CDK5), in turn, promote Rb1 hyperphosphorylation, which activates E2F1, and E2F1 promotes of NED and proliferation in C4-2b-ENZR and NCI-H660 by stimulation of NED gene expression in addition to E2F1-regulated genes required for cell-cycle progression.

PARP inhibitors suppress N-Myc–mediated, RB1–independent, and -dependent NED signaling

We investigated the impact of PARP inhibition on N-Myc-dependent, RB1-independent, and RB1-dependent NED signaling using C4-2b, C4-2b-ENZR, and NCI-H660 cells. Our results showed inhibition of PARP by OLA or TALA (another PARP inhibitor) led to downregulation of N-Myc protein and marked downregulation of expression of CDK5R1, CDK5R2, Rb1 phosphorylation at S807/811 (target of CDKs 1, 2, 4, 5, 6, and 9) and S780 (target of CDKs 4 and 6), and NED markers (CHGA, SYP, and NSE protein; Fig. 5A). To test the effects of OLA and TALA in an NEPC organoid model, we used MSKCC PCa4, and initially confirmed expression of MYCN-CDK5R1/CDK5R2 (CDK5)–RB1–E2F1 signaling pathway genes relative to C4-2b, C4-2b-ENZR, and NCI-H660 cells (Fig. 5B). Treatment of MSKCC PCa4 organoids showed suppression of the MYCN–CDK5–RB1–E2F1 signaling pathway (Fig. 5C). IHC analysis confirmed OLA and TALA suppression of Rb1 phosphorylation in C4-2b, C4-2b-ENZR, and NCI-H660 cells (Fig. 5D–F). ChIP-qPCR assays demonstrated that PARP inhibition significantly suppressed GR binding to BS1 on the MYCN promoter (Fig. 5G), N-Myc binding to BS2 on CDK5R1, and BS1 and BS4 on CDK5R2 (Fig. 5H). PARP inhibition also significantly suppressed N-Myc and E2F1 binding to CHGA, SYP, and NSE (Fig. 5I). GSEA analysis indicated that OLA significantly suppressed ENZ-stimulated E2F target gene expression (ENZ vs. ENZ+OLA) in MDA prostate cancer PDX133-4 T2 tumors (Supplementary Fig. S9). Our data are consistent with previous findings that PARP1 functions as an E2F1 coactivator that promotes transcription of E2F1 target genes (42–44).

PARP inhibitor and CDK5 inhibitor combination treatment significantly improves therapy efficacy

On the basis of these data, we speculated that maximal inhibition of GR–MYCN–CDK5–RB1–E2F–NED signaling pathway could be achieved by the combination PARP inhibition and CDK5 inhibition. To test this hypothesis, we tested OLA+DINA combination therapy using C4-2b-ENZR and NCI-H660 cells *in vitro* and MDA prostate cancer PDX144-13 and NCI-H660 xenograft models. Targeted genomic DNA sequencing revealed a TP53 frame shift mutation L330fs and a RB1 frame shift mutation V450fs in MDA prostate cancer PDX144-13 (Supplementary Fig. S1; Supplementary Table S1). Our *in vitro* data demonstrated that although OLA or DINA alone could significantly increase apoptosis, indicated by increased sub-G_1 cells (Fig. 6A and B), and significantly reduce cell viability (Fig. 6C and D), the OLA and DINA combination treatment further improved therapeutic efficiency significantly (Fig. 6A–D). Our *in vivo* results showed that OLA or DINA alone could efficiently suppress NEPC tumor growth (about 35%–55% tumor suppression), whereas the OLA and DINA combination led to significantly greater tumor suppression (~80% tumor suppression. PDX 144-6: OLA+DINA vs. OLA $P = 0.042$, OLA+DINA vs. DINA $P =$

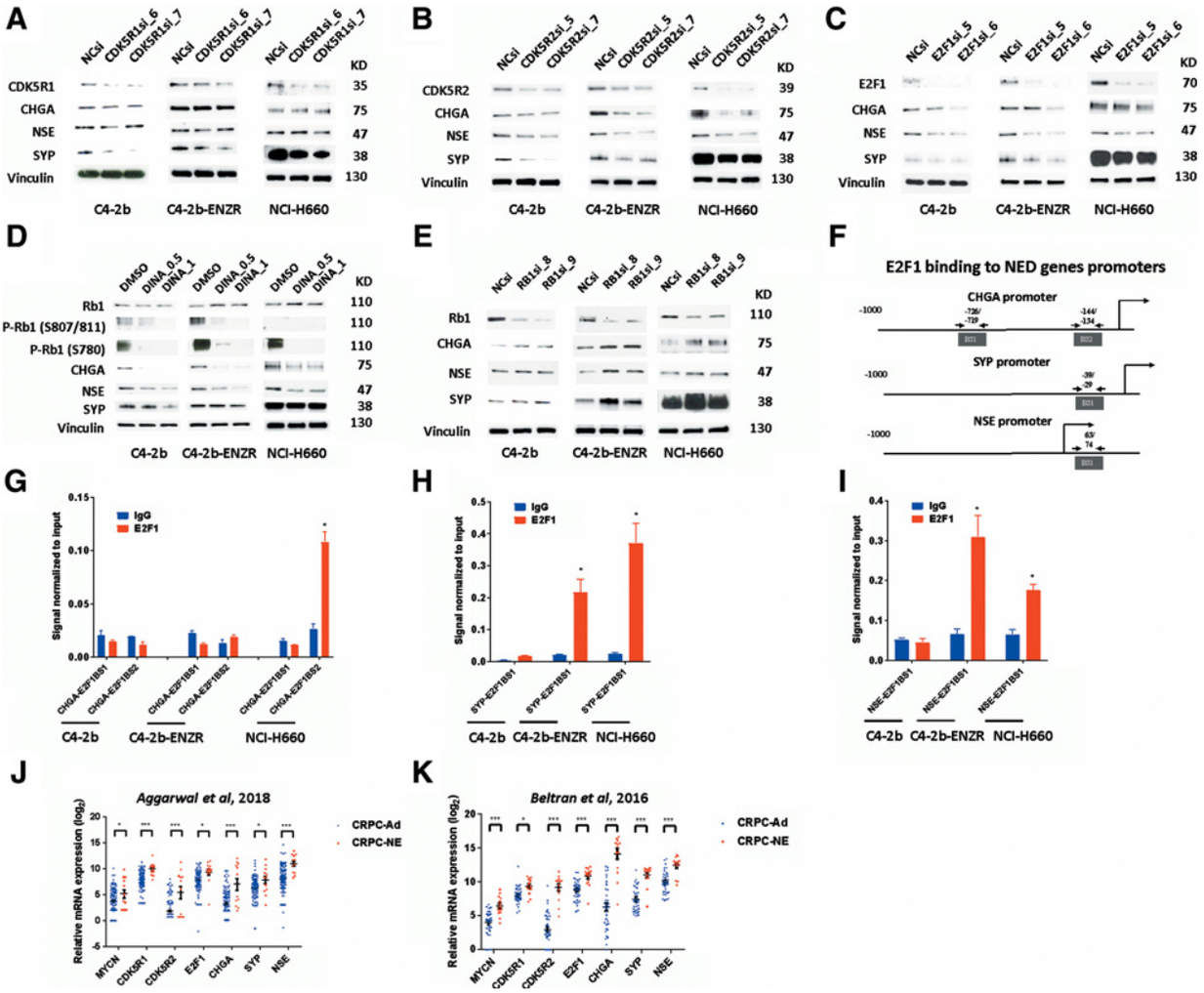

Figure 4.

CDK5R1, CDK5R2, Rb1 phosphorylation, and E2F1 positively regulate expression of NED markers. Effect of CDK5R1si (**A**), CDK5R2si (**B**), and E2F1si (**C**) on protein expression of CHGA, SYP, and NSE in C4-2b, C4-2b-ENZR, and NCI-H660 cells. **D,** CDK5 inhibition with DINA suppressed Rb1 phosphorylation and expression of CHGA, SYP, and NSE in C4-2b, C4-2b-ENZR, and NCI-H660 cells 48 hours after the treatment. DINA_0.5, DINA 0.5 μmol/L; DINA_1, DINA 1 μmol/L; **E,** Knockdown of RB1 led to increased protein expression of CHGA, SYP, and NSE in C4-2b, C4-2b-ENZR, and NCI-H660 cells. **F,** Predicted E2F1 binding sites on CHGA, SYP, and NSE promoter according to JASPAR database. **G–I,** ChIP-qPCR analysis testing the direct binding of E2F1 to CHGA, SYP, and NSE promoters in C4-2b, C4-2b-ENZR, and NCI-H660. **J** and **K,** Relative expression levels of MYCN, CDK5R1, CDK5R2, E2F1, CHGA, SYP, and NSE of CRPC-Ad and CRPC-NE in Aggarwal and colleagues' and Beltran and colleagues' datasets. *, $P < 0.05$; **, $P < 0.01$; ***, $P < 0.001$.

0.045; NCI-H660: OLA+DINA vs. OLA $P = 2.73$ E-6, OLA+DINA vs. DINA $P = 0.003$; Fig. 6E–H). IHC analysis of tumor samples demonstrated reduced P-Rb1 phosphorylation and CHGA and SYP positivity (Fig. 6I), increased apoptotic activity (TUNEL), and decreased proliferation (Ki67; Supplementary Fig. S10) in OLA or DINA treated tumor samples compared with VHL tumor samples, and further enhanced treatment effects in OLA+DINA tumors.

Importantly, PARP inhibition deactivates the GR–MYCN axis by downregulation of GR-activated MYCN expression, which leads to both direct suppression of N-Myc transcriptional upregulation of E2F1, and downstream CDK5–RB1–E2F1 signaling, to inhibit NED and proliferation of ENZ-treated prostate cancer cells, and NEPC (Fig. 6J). To further validate the functionality of GR vis-à-vis induction of this pathway, we used an inducible GR-DU145 cell line. The results of GR induction demonstrated activation of MYCN–CDK5–RB1–E2F1–NED signaling *in vitro* in prostate cancer cells (Supplementary Fig. S11).

Discussion

NEPC is currently considered to be an incurable disease. The difficulty in treatment is fundamentally because of lack of understanding of molecular mechanisms underlying development of NEPC, and lack of available treatment options which target the NEPC-related resistance pathways that render conventional treatment approaches ineffective. In this study, we demonstrated that long-term ENZ treatment led to NED, and PARP inhibitors, well-established DDR targeting agents, suppressed ENZ-related NED.

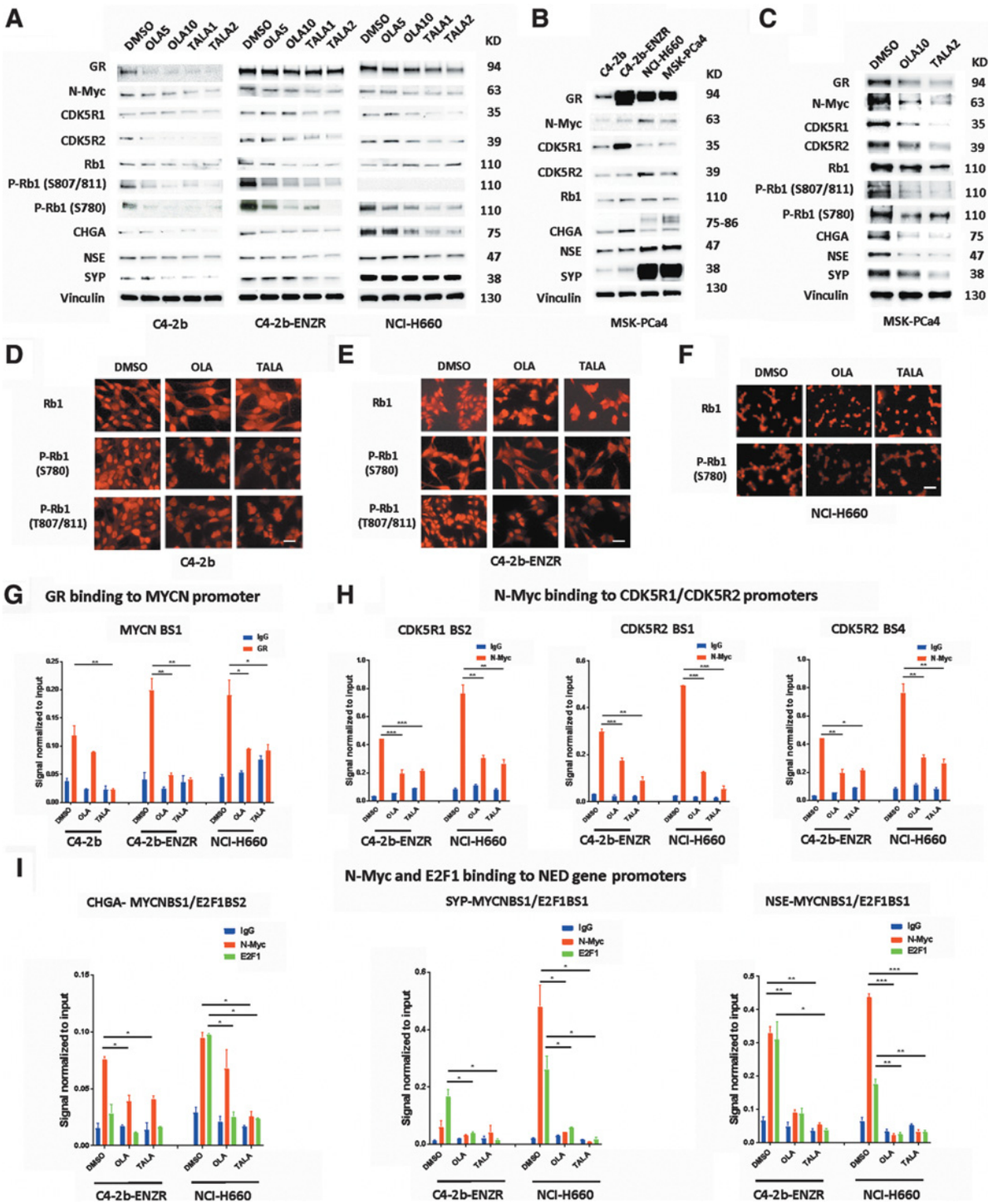

Figure 5.

PARP inhibitors suppress the GR–MYCN–CDK5–RB1–E2F1–NED signaling pathway. **A,** Effect of OLA and TALA on protein expression of N-Myc, CDK5R1, CDK5R2, P-Rb1, and NED genes in C4-2b, C4-2b-ENZR, and NCI-H660 cells 48 hours after the treatments. OLA5, OLA 5 μmol/L; OLA10, OLA 10 μmol/L; TALA1, TALA 1 μmol/L; TALA2, TALA 2 μmol/L. **B,** GR-MYCN-CDK5 pathway protein expression in MSK PCa4 organoid line. **C,** GR–MYCN–CDK5 pathway protein expression in response to PARP inhibition (OLA 5 μmol/L, TALA 2 μmol/L) in MSK PCa4 organoid line. **D–F,** IHC analysis showing weaker P-Rb1 (S807/811) and P-Rb1 (S780) staining in OLA 5 μmol/L-treated, TALA 2 μmol/L-treated C4-2b and C4-2b-ENZR cells, and weaker P-Rb1 (S780) staining in OLA, TALA-treated NCI-H660 cells. Scale bar represents 50 μm. **G–I,** ChIP-qPCR analysis testing the direct binding of GR, N-Myc, and E2F1 to NED genes and its suppression by PARP inhibitors (OLA 5 μmol/L, TALA 2 μmol/L). *, $P < 0.05$; **, $P < 0.01$; ***, $P < 0.001$.

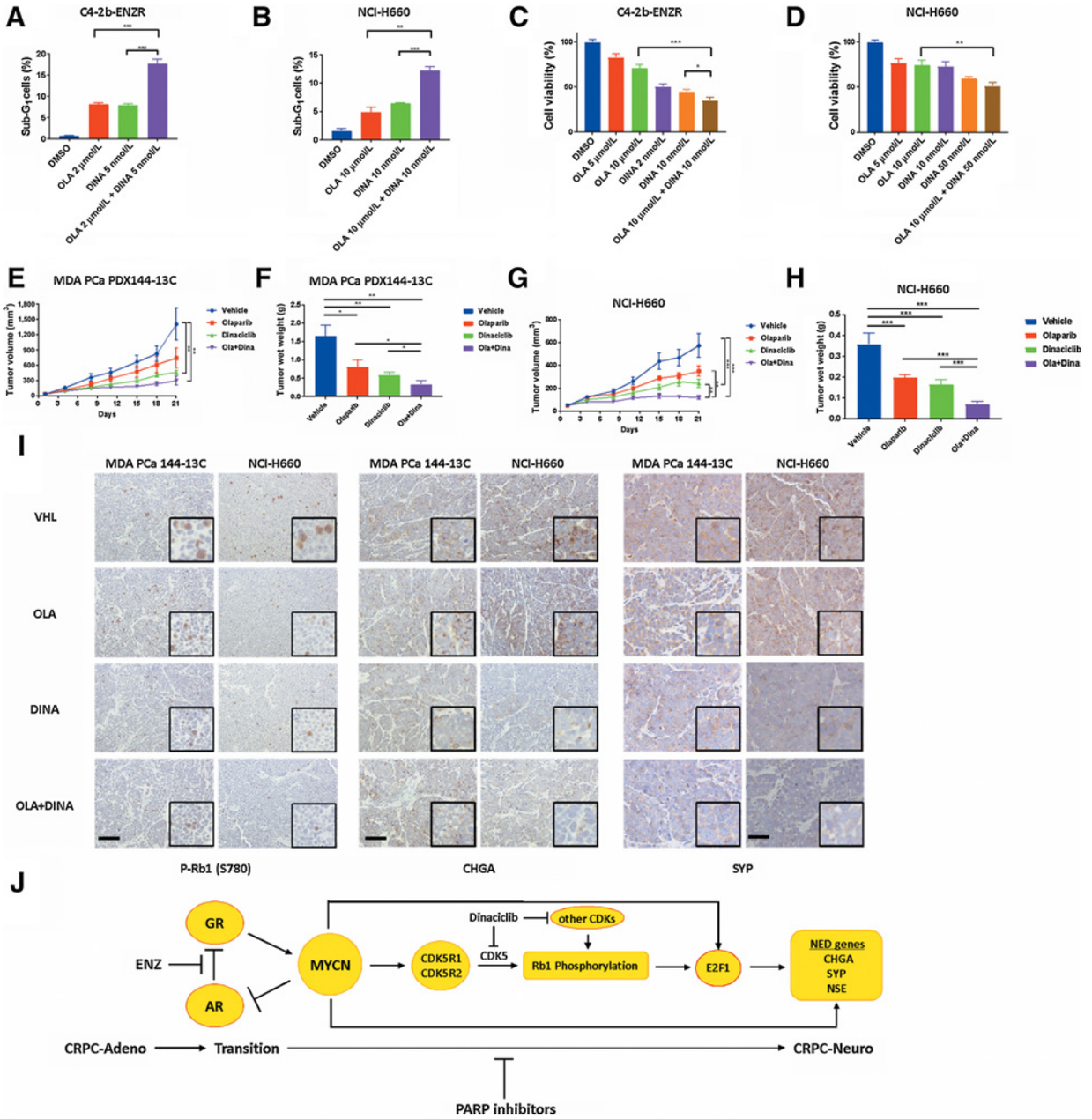

Figure 6.

PARP and CDK5 inhibition cooperatively suppress prostate cancer oncogenic activities *in vitro* and xenograft tumor growth *in vivo*. **A** and **B,** Effect of OLA, DINA, and combination of OLA and DINA on sub-G_1 cell distribution in C4-2b-ENZR and NCI-H660 cells. **C** and **D,** MTS assays showing effect of OLA, DINA, and combination of OLA and DINA on cell proliferation/viability in C4-2b-ENZR and NCI-H660 cells. **E–H,** Results from MDA prostate cancer PDX144-13C and NCI-H660 subcutaneous model. **E,** Tumor growth curve for MDA prostate cancer PDX144-13C. **F,** Tumor wet weight for MDA prostate cancer PDX144-13C. **G,** Tumor growth curve for NCI-H660. **H,** Tumor wet weight for NCI-H660. **I,** IHC analysis showing suppression of P-Rb1(S780), CHGA, and SYP by OLA, DINA, and OLA+DINA in MDA prostate cancer PDX144-13C and NCI-H660 xenograft tumors. Scale bar represents 150 μm. **J,** ENZ-stimulated GR–MYCN–CDK5–RB1–E2F1–NED signaling pathway, and its suppression by PARP inhibition. *, $P < 0.05$; **, $P < 0.01$; ***, $P < 0.001$.

Progressive loss of AR target gene activation, together with increased GR expression was shown previously to represent an adaptive, bypass mechanism of resistance to AR signaling inhibitors (3). Our results expand the scope of this adaptive mechanism to include activation of a molecular gateway to NED through GR transcriptional regulation of *MYCN*, that is, the GR–N-Myc axis. Our results demonstrated that increased *MYCN* expression can, in turn, directly stimulate NED gene expression through transcriptional activation, supporting previously described work (5), and also initiate RB1-dependent, E2F1-

mediated NED signaling which can serve to release the constraints on lineage plasticity without RB1 mutation or deletion.

In this study, we showed that CDK5R1/R2 and CDK5 activities, and likely CDK2, CDK4, and CDK6 activities, are critical regulators of a functional Rb1 switch that controls NED through E2F1 transcriptional regulation of NED gene expression, including CHGA, SYP, and NSE. On the basis of our findings, the role of CDK5R1/R2 and CDK5 in NEPC warrants further study. In addition to regulation of E2F1 through transactivation of CDK5R1/R2 and Rb1 inactivation, N-Myc can directly bind and transactivate E2F1, further enhancing E2F1-mediated NED gene transcription. It is interesting to note that loss of RB results in E2F1 repositioning and expansion of E2F1 cistrome (45). Specifically, E2F1 was shown to lack affinity for CHGA, SYP, and ENO2 (NSE) in LNCaP shCON cells, but showed strong binding to these 3 genes in LNCaP shRB cells. Furthermore, N-Myc tends to colocalize with E2F1 on these 3 NED genes (Fig. 5F; Supplementary Fig. S4A). The significance of the colocalization of these 2 transcription factors on NED genes warrants further study. Overall, elucidation of the GR–MYCN–CDK5R1/R2–RB1–E2F1–NED molecular pathway connects ENZ-associated increased GR expression with MYCN transactivation, Rb1 inactivation, and NED, in the absence of *Rb1* mutation or deletion. It is important to note that we also documented that the MDA PCa PDX133-4 model and C4-2b-ENZR, but not parental C4-2b cells harbor functional TP53 mutations (Supplementary Fig. S1). These findings support cooperative functions of Rb1 and TP53 mutations in driving ENZ treatment—associated NED. Our results have obvious implications for interpretation of pathologic information from patients with prostate cancer who receive AR signaling inhibitor therapy, and for the development of prognostic and predictive biomarkers for patients with prostate cancer in a transition state prior to the development of NEPC and small cell prostate cancer with *Rb1* and TP53 genomic alterations.

A clinically important finding of our study was that PARP inhibition suppresses development of NED through inhibiting the GR–MYCN–CDK5R1/R2–RB1–NED molecular pathway. We demonstrated that PARP inhibitors suppress GR-mediated transcriptional regulation of *MYCN*, N-Myc-mediated transcriptional regulation of NED genes and *CDK5R1/R2*, and E2F1-mediated transcriptional regulation of *CHGA*, *SYP*, and *NSE* (presumably also E2F1-mediated transcriptional regulation of cell cycle-promoting genes). Although unexpected, these results are consistent with the well-documented role of PARP in the transcriptional regulation of multiple genetic pathways including cell differentiation (46, 47). PARP-mediated transcriptional regulation activities are linked to chromatin modification, thus within the context of NEPC, further analysis of chromatin modification together with PARP regulation of the GR–MYCN–CDK5R1/R2–RB1–NED molecular pathway is warranted. Importantly, elucidation of PARP-mediated transcriptional regulation of the GR–MYCN–CDK5R1/R2–RB1–NED molecular pathway exposes therapeutic vulnerabilities with regard to targeting lineage plasticity, and the development of NED and NEPC. To validate the clinical implications of our study we showed that OLA+DINA treatment suppressed growth of NEPC xenograft models and, importantly reduced NED in tumor tissues *in vivo*. Additional preclinical studies that leverage PARP inhibitor-mediated transcriptional suppression of key nodes in the GR–MYCN–CDK5R1/R2–RB1–NED molecular pathway are warranted. In addition, studies that test combination treatment approaches that include PARP inhibitors and CDK inhibitors that prevent phosphorylation (inactivation) of Rb1 may lead to more effective therapies for NEPC.

In summary, the results of our study indicate an important role of GR–MYCN–CDK5R1/2–RB1–NED signaling in ENZ-induced and OLA-suppressed NEPC. We also demonstrated efficacy for OLA+DINA combination therapy in NEPC xenograft models. Further investigation of treatment related NEPC in light of our findings will hopefully lead to effective therapies for this currently incurable disease.

Disclosure of Potential Conflicts of Interest

H. Beltran is an unpaid consultant/advisory board member of Janssen and Astellas. M.T. Tetzlaff is an unpaid consultant/advisory board member of Myriad Genetics, Seattle Genetics, Novartis LLC, and Nanostring. No potential conflicts of interest were disclosed by the other authors.

Authors' Contributions

Conception and design: B. Liu, L. Li, G. Yang, C. Geng, Z. Tang, C. Wu, T.C. Thompson

Development of methodology: B. Liu, L. Li, G. Yang, C. Geng, Y. Luo, D. Korentzelos, Z. Tang, C. Wu, Y. Chen, M.T. Tetzlaff, T.C. Thompson

Acquisition of data (provided animals, acquired and managed patients, provided facilities, etc.): B. Liu, L. Li, G. Yang, C. Geng, Y. Luo, D. Korentzelos, S. Park, Z. Tang, C. Wu, H. Beltran, M.T. Tetzlaff, P. Troncoso, T.C. Thompson

Analysis and interpretation of data (e.g., statistical analysis, biostatistics, computational analysis): B. Liu, L. Li, G. Yang, C. Geng, Y. Luo, W. Wu, G.C. Manyam, D. Korentzelos, Z. Tang, C. Wu, M. Sigouros, A. Sboner, H. Beltran, P. Troncoso, B. Broom, T.C. Thompson

Writing, review, and/or revision of the manuscript: B. Liu, L. Li, G. Yang, C. Geng, Z. Tang, C. Wu, P.G. Corn, M.T. Tetzlaff, P. Troncoso, B. Broom, T.C. Thompson

Administrative, technical, or material support (i.e., reporting or organizing data, constructing databases): G. Yang, C. Geng, Y. Luo, Z. Tang, C. Wu, Z. Dong, M. Sigouros, Y. Chen, T.C. Thompson

Study supervision: B. Broom, T.C. Thompson

Acknowledgments

This research was supported by MD Anderson NCI Prostate Cancer SPORE Grant P50 CA140388, and the NCI Cancer Center Support Grant P30 CA16672.

The costs of publication of this article were defrayed in part by the payment of page charges. This article must therefore be hereby marked *advertisement* in accordance with 18 U.S.C. Section 1734 solely to indicate this fact.

Received January 25, 2019; revised April 25, 2019; accepted August 15, 2019; published first August 22, 2019.

References

1. de Bono JS, Logothetis CJ, Molina A, Fizazi K, North S, Chu L, et al. Abiraterone and increased survival in metastatic prostate cancer. N Engl J Med 2011;364:1995–2005.
2. Scher HI, Fizazi K, Saad F, Taplin ME, Sternberg CN, Miller K, et al. Increased survival with enzalutamide in prostate cancer after chemotherapy. N Engl J Med 2012;367:1187–97.
3. Arora VK, Schenkein E, Murali R, Subudhi SK, Wongvipat J, Balbas MD, et al. Glucocorticoid receptor confers resistance to antiandrogens by bypassing androgen receptor blockade. Cell 2013;155:1309–22.
4. Palmgren JS, Karavadia SS, Wakefield MR. Unusual and underappreciated: small cell carcinoma of the prostate. Semin Oncol 2007;34:22–9.

5. Beltran H, Rickman DS, Park K, Chae SS, Sboner A, MacDonald TY, et al. Molecular characterization of neuroendocrine prostate cancer and identification of new drug targets. Cancer Discov 2011;1:487–95.
6. Mosquera JM, Beltran H, Park K, MacDonald TY, Robinson BD, Tagawa ST, et al. Concurrent AURKA and MYCN gene amplifications are harbingers of lethal treatment-related neuroendocrine prostate cancer. Neoplasia 2013; 15:1–10.
7. Aggarwal R, Huang J, Alumkal JJ, Zhang L, Feng FY, Thomas GV, et al. Clinical and genomic characterization of treatment-emergent small-cell neuroendocrine prostate cancer: a multi-institutional prospective study. J Clin Oncol 2018;36:2492–503.
8. Beltran H, Prandi D, Mosquera JM, Benelli M, Puca L, Cyrta J, et al. Divergent clonal evolution of castration-resistant neuroendocrine prostate cancer. Nat Med 2016;22:298–305.
9. Dardenne E, Beltran H, Benelli M, Gayvert K, Berger A, Puca L, et al. N-Myc induces an EZH2-mediated transcriptional program driving neuroendocrine prostate cancer. Cancer Cell 2016;30:563–77.
10. Lee JK, Phillips JW, Smith BA, Park JW, Stoyanova T, McCaffrey EF, et al. N-Myc drives neuroendocrine prostate cancer initiated from human prostate epithelial cells. Cancer Cell 2016;29:536–47.
11. Chinnam M, Goodrich DW. RB1, development, and cancer. Curr Top Dev Biol 2011;94:129–69.
12. Rodrigues DN, Boysen G, Sumanasuriya S, Seed G, Marzo AM, de Bono J. The molecular underpinnings of prostate cancer: impacts on management and pathology practice. J Pathol 2017;241:173–82.
13. Soundararajan R, Aparicio AM, Logothetis CJ, Mani SA, Maity SN. Function of tumor suppressors in resistance to antiandrogen therapy and luminal epithelial plasticity of aggressive variant neuroendocrine prostate cancers. Front Oncol 2018;8:69.
14. Akamatsu S, Inoue T, Ogawa O, Gleave ME. Clinical and molecular features of treatment-related neuroendocrine prostate cancer. Int J Urol 2018;25: 345–51.
15. Ku SY, Rosario S, Wang Y, Mu P, Seshadri M, Goodrich ZW, et al. Rb1 and Trp53 cooperate to suppress prostate cancer lineage plasticity, metastasis, and antiandrogen resistance. Science 2017;355:78–83.
16. Mu P, Zhang Z, Benelli M, Karthaus WR, Hoover E, Chen CC, et al. SOX2 promotes lineage plasticity and antiandrogen resistance in TP53- and RB1-deficient prostate cancer. Science 2017;355:84–8.
17. Park JW, Lee JK, Sheu KM, Wang L, Balanis NG, Nguyen K, et al. Reprogramming normal human epithelial tissues to a common, lethal neuroendocrine cancer lineage. Science 2018;362:91–5.
18. Ellisen LW. PARP inhibitors in cancer therapy: promise, progress, and puzzles. Cancer Cell 2011;19:165–7.
19. Castro E, Mateo J, Olmos D, de Bono JS. Targeting DNA repair: the role of PARP inhibition in the treatment of castration-resistant prostate cancer. Cancer J 2016;22:353–6.
20. Li L, Chang W, Yang G, Ren C, Park S, Karantanos T, et al. Targeting poly (ADP-ribose) polymerase and the c-Myb-regulated DNA damage response pathway in castration-resistant prostate cancer. Sci Signal 2014;7:ra47.
21. Li L, Karanika S, Yang G, Wang J, Park S, Broom BM, et al. Androgen receptor inhibitor-induced "BRCAness" and PARP inhibition are synthetically lethal for castration-resistant prostate cancer. Sci Signal 2017;10. pii: eaam7479.
22. Zhang W, Liu B, Wu W, Li L, Broom BM, Basourakos SP, et al. Targeting the MYCN-PARP-DNA damage response pathway in neuroendocrine prostate cancer. Clin Cancer Res 2018;24:696–707.
23. Gao D, Vela I, Sboner A, Iaquinta PJ, Karthaus WR, Gopalan A, et al. Organoid cultures derived from patients with advanced prostate cancer. Cell 2014;159:176–87.
24. Navone NM, Labanca E. Modeling cancer metastasis. In: Wang Y, Lin D, Gout PW eds. Patient-derived xenograft models of human cancer. Humana Press 2017:93–114.
25. Conway T, Wazny J, Bromage A, Tymms M, Sooraj D, Williams ED, et al. Xenome–a tool for classifying reads from xenograft samples. Bioinformatics 2012;28:i172–8.
26. Kim D, Pertea G, Trapnell C, Pimentel H, Kelley R, Salzberg SL. TopHat2: accurate alignment of transcriptomes in the presence of insertions, deletions and gene fusions. Genome Biol 2013;14:R36.
27. Li H, Handsaker B, Wysoker A, Fennell T, Ruan J, Homer N, et al. The Sequence Alignment/Map format and SAMtools. Bioinformatics 2009;25: 2078–9.
28. Anders S, Pyl PT, Huber W. HTSeq–a Python framework to work with high-throughput sequencing data. Bioinformatics 2015;31:166–9.
29. Love MI, Huber W, Anders S. Moderated estimation of fold change and dispersion for RNA-seq data with DESeq2. Genome Biol 2014;15:550.
30. Beltran H, Wyatt AW, Chedgy EC, Donoghue A, Annala M, Warner EW, et al. Impact of therapy on genomics and transcriptomics in high-risk prostate cancer treated with neoadjuvant docetaxel and androgen deprivation therapy. Clin Cancer Res 2017;23:6802–11.
31. Hieronymus H, Lamb J, Ross KN, Peng XP, Clement C, Rodina A, et al. Gene expression signature-based chemical genomic prediction identifies a novel class of HSP90 pathway modulators. Cancer Cell 2006;10:321–30.
32. Xu H, El-Gewely MR. Differentially expressed downstream genes in cells with normal or mutated p53. Oncol Res 2003;13:429–36.
33. Li W, Allen ME, Rui Y, Ku L, Liu G, Bankston AN, et al. p39 Is responsible for increasing Cdk5 activity during postnatal neuron differentiation and governs neuronal network formation and epileptic responses. J Neurosci 2016;36:11283–94.
34. Kesavapany S, Li BS, Amin N, Zheng YL, Grant P, Pant HC. Neuronal cyclin-dependent kinase 5: role in nervous system function and its specific inhibition by the Cdk5 inhibitory peptide. Biochim Biophys Acta 2004; 1697:143–53.
35. Hisanaga S, Endo R. Regulation and role of cyclin-dependent kinase activity in neuronal survival and death. J Neurochem 2010;115:1309–21.
36. Arif A. Extraneuronal activities and regulatory mechanisms of the atypical cyclin-dependent kinase Cdk5. Biochem Pharmacol 2012;84:985–93.
37. Lee KY, Helbing CC, Choi KS, Johnston RN, Wang JH. Neuronal Cdc2-like kinase (Nclk) binds and phosphorylates the retinoblastoma protein. J Biol Chem 1997;272:5622–6.
38. Futatsugi A, Utreras E, Rudrabhatla P, Jaffe H, Pant HC, Kulkarni AB. Cyclin-dependent kinase 5 regulates E2F transcription factor through phosphorylation of Rb protein in neurons. Cell Cycle 2012;11: 1603–10.
39. Pozo K, Castro-Rivera E, Tan C, Plattner F, Schwach G, Siegl V, et al. The role of Cdk5 in neuroendocrine thyroid cancer. Cancer Cell 2013;24:499–511.
40. Williams BO, Remington L, Albert DM, Mukai S, Bronson RT, Jacks T. Cooperative tumorigenic effects of germline mutations in Rb and p53. Nat Genet 1994;7:480–4.
41. Takahashi C, Contreras B, Iwanaga T, Takegami Y, Bakker A, Bronson RT, et al. Nras loss induces metastatic conversion of Rb1-deficient neuroendocrine thyroid tumor. Nat Genet 2006;38:118–23.
42. Schiewer MJ, Mandigo AC, Gordon N, Huang F, Gaur S, de Leeuw R, et al. PARP-1 regulates DNA repair factor availability. EMBO Mol Med 2018;10. doi:10.15252/emmm.201708816.
43. Simbulan-Rosenthal CM, Rosenthal DS, Luo R, Samara R, Espinoza LA, Hassa PO, et al. PARP-1 binds E2F-1 independently of its DNA binding and catalytic domains, and acts as a novel coactivator of E2F-1-mediated transcription during re-entry of quiescent cells into S phase. Oncogene 2003;22:8460–71.
44. Byers LA, Wang J, Nilsson MB, Fujimoto J, Saintigny P, Yordy J, et al. Proteomic profiling identifies dysregulated pathways in small cell lung cancer and novel therapeutic targets including PARP1. Cancer Discov 2012;2:798–811.
45. McNair C, Xu K, Mandigo AC, Benelli M, Leiby B, Rodrigues D, et al. Differential impact of RB status on E2F1 reprogramming in human cancer. J Clin Invest 2018;128:341–58.
46. Schreiber V, Dantzer F, Ame JC, de Murcia G. Poly(ADP-ribose): novel functions for an old molecule. Nat Rev Mol Cell Biol 2006;7:517–28.
47. Bock FJ, Chang P. New directions in poly(ADP-ribose) polymerase biology. FEBS J 2016;283:4017–31.